Double-Layer Energy Management for Multi-Motor Electric Vehicles

Binh-Minh Nguyen, *Member, IEEE*, João Pedro F. Trovão, *Senior Member*, *IEEE*, Minh C. Ta, *Senior Member*, *IEEE*

***Abstract* – This paper proposes a double-layer energy management system (EMS) for electric vehicles driven by multiple permanent magnet synchronous motors. The system minimizes energy consumption and ensures safe longitudinal motion. The inner-layer distributes torques and flux currents by minimizing the motor input power. The outer-layer generates the total torque command by controlling the aggregated motor speed via a disturbance observer-based controller. A design condition that sufficiently guarantees the system's L_2 stability is presented. The condition is independent of the torque distribution ratios and can be checked conveniently via passivity notation without linearizing the total system. Various validation tests were performed using a three-wheel recreational electric vehicle (EV) platform. The advantage of the double-layer EMS has been compared with several EMSs proposed recently in the literature. Critical testing scenarios were employed, including sharp change in road friction during high acceleration. Test results reveal that, regardless of such condition, the double-layer EMS can prevent the wheel slip, thereby significantly reducing energy consumption. The New European Driving Cycle test was also conducted to demonstrate the merit of simultaneously optimizing torque distribution ratios and motor flux-currents.**

***Index Terms* - Electric vehicle, energy management system, multi-motor, passivity, anti-slip, disturbance observer.**

I. Introduction

AN ELECTRIC VEHICLE (EV) is a system that exchanges the energy between the sources and the motors [1]. In recent years, both sides have been developed as multi-unit systems, which has encouraged the study on energy management systems (EMSs) [2] – [3]. This paper examines the EMSs for motor side, in which the motors are of the permanent magnet synchronous motor (PMSM) type. As summarized in TABLE I, several main concepts have been proposed, namely (I) tire-force distribution (TFD) [4] – [9], (II) torque vectoring control (TVC) [10]–[16], and (III) front-rear torque distribution (FRTD) [17] – [23]. Investigating the aforementioned studies, we have recognized several issues.

First, almost all the methods in TABLE I do not have the capability of wheel-slip prevention. The wheel-slip phenomenon results in significant energy loss, especially when the EV operates on the low friction surface [1]. In an attempt to combine energy optimization and safe traction, an EMS was proposed in [23] by providing a disturbance observer (DOB) based anti-slip controller for each controlled wheel. However, the anti-slip control signals appear in the cost function of the energy optimization problem in [23]. This increases the complexity of the EMS algorithm, and only enables the numerical calculation of the optimal torque distribution ratios. To reduce the computational burden, it is essential to develop an EMS that allows the energy optimization and the slip prevention to be performed simultaneously but independently.

Second, a practical approach to system stabilization is still a challenge. Due to nonlinear tire force characteristics [24], the EV is actually a complex dynamical system. An attempt to stabilize the FRTD system was performed in [18]. However, this study merely treated the vehicle system as four independent wheel speed control loops. This modelling is too simplified to capture the real dynamics of the EV. Moreover, the stability analysis in [18] relies on the torque distribution ratios, which are time-varying variables. To alleviate the computational burden, we aim to seek a design condition that is free from the torque distribution ratios and the linearization process.

Third, it is still necessary to formulate motor input power as a function of both torque distribution ratios and motor flux-currents. This objective function has not been considered by almost all the methods summarized in TABLE I. For instance, TVC methods commonly address the minimization of powertrain's power loss via torque distribution. The FRTD methods [17] – [19] obtained motor input power as a quadratic function of the distribution ratios. Unfortunately, this objective function was merely derived under the assumption that the PMSMs' flux currents were zero. However, the flux current of the PMSM should be controlled at a certain value, depending on the motor speed, to reduce power loss [25].

To deal with the aforementioned issues, this paper focuses on the general multi-motor EV prototype in which each wheel is driven by a PMSM. A double-layer EMS is proposed to minimize energy consumption and guarantees safe longitudinal motion. The inner-layer distributes the torques and flux currents by minimizing the motor input power. The inner-layer

This work was supported in part by Kurata Grants from the Hitachi Global Foundation, KAKENHI-PROJECT-22K14283, Research Grant Program from New Energy and Industrial Technology Development Organization (NEDO) of Japan (No. 05A48701d), Grant 950-230672 from Canada Research Chairs Program, and Grant RGPIN-2017-05924 from the Natural Sciences and Engineering Research Council of Canada.

Binh-Minh Nguyen is with the Department of Advanced Energy, The University of Tokyo, Bunkyo, Tokyo, Japan (e-mail: nguyen.binhminh@edu.k.u-tokyo.ac.jp). João Pedro F. Trovão is with the Department of Electrical Engineering and Computer Engineering, University of Sherbrooke, Sherbrooke, QC, J1K 2R1, Canada, and also with the IPC-ISEC Coimbra, 3030-290 Coimbra, Portugal (e-mail: joao.trovao@usherbrooke.ca). Minh C. Ta is with the Department of Electrical Engineering and Computer Engineering, University of Sherbrooke, Sherbrooke, QC, J1K 2R1, Canada, and also with School of Electrical and Electronic Engineering, Hanoi University of Science and Technology, Vietnam (e-mail: cao.minh.ta@usherbrooke.ca).

TABLE I
LITERATURE REVIEW ON THE METHODS TO DEVELOP MOTOR SIDE EMS

Concept	Scheme	Pros	Cons	Ref. No.
(I) Tire force distribution	Minimization of the squared sum of tire slip energy dissipation rate or tire workload.	Directly related to the performance of the vehicle dynamics with the consideration of both lateral and longitudinal motion.	Lack the wheel-slip prevention function, the stability analysis, and the consideration of motor input energy.	[4], [5], [6] [7], [8], [9]
(II) Torque vectoring control	Integration of direct yaw moment control with torque distribution to minimize the powertrain's power loss.	Simultaneously reduce the powertrain's loss and improve the lateral stability of the vehicle.	Lack the motor flux-current optimization and practical stability condition of the overall system.	[10], [11], [12] [13], [14], [15], [16]
(III) Front-rear torque distribution →*Aim of this paper to improve.*	Minimization of motor input power using on-line torque distribution.	Convenient for implementing in real-time applications; Optimal torque distribution ratios can be calculated in advance for a given speed pattern.	Lack the wheel-slip prevention function, the stability analysis of the overall system, and the investigation of the motor flux-current.	[17], [18], [19], [20]
	Energy-efficient torque allocation using off-line optimization.			[21]
	Integration of optimal torque distribution with sliding-mode based wheel-slip ratio control.	The method can reduce the energy loss due to wheel slip.	The anti-slip control signal interferes the energy optimization algorithm.	[22]
	Integration of optimal torque distribution with disturbance observer based anti-slip control.	The method can reduce the energy loss due to wheel slip. In addition, a stability condition is established.	The anti-slip control signal interferes the energy optimization algorithm.	[23]

also provides an aggregated speed of the motors using the torque distribution ratios. In the outer-layer, the aggregated motor speed is controlled by a DOB based controller. Based on passivity theory [26], a design condition that sufficiently guarantees L_2 stability of the control system is established. In other words, this paper generalizes the idea of applying passivity to EMS, which was briefly introduced in [23] and [27]. The main contributions of this paper can be considered as follows:

(i) This paper presents a new configuration for combining EMS with anti-slip control. The proposed configuration has only one DOB-based controller that controls the aggregated motor speed. Thanks to this configuration, the DOB control signal does not intervene the energy optimization problem, as in [23]. Hence, energy optimization and slip prevention algorithms can be designed independently.

(ii) This paper presents a convenient and practical approach to stabilizing the overall system. Unlike [18], the stability condition does not rely on torque distribution ratios, which are time-varying variables used to minimize the motor input power. Furthermore, there is no need to linearize the EV dynamics.

(iii) This paper formulates the summation of motor output powers with copper losses and iron losses as a function of torque distribution ratios and motor flux-current. The minimization of this cost function allows instantaneous efficiency optimization in the inner-layer, together with anti-slip control in the outer-layer.

The remainder of this paper is organized as follows. The dynamics of the multi-motor EV and the energy model are presented in Section II. Section III briefly introduces the passivity theory and analyzes the passivity property of the EV's longitudinal dynamics. The double-layer EMS, the energy optimization problem, and the passivity-based design condition are presented in Section IV. Using a three-wheel recreational EV platform, a design example is presented in Section V. Test results are demonstrated in Section VI by comparing the double-layer EMS with several EMSs recently proposed in the literature. Finally, the conclusion and future works are presented in Section VII.

II. VEHICLE DYNAMICS AND ENERGY MODEL

To describe the *N*-wheel-EV model (*N* is a positive integer), the main nomenclatures are summarized in TABLE II.

TABLE II
NOMENCLATURE

v_x	Longitudinal speed of the vehicle body
m	Total mass of the vehicle
COG	Center of gravity
σ	Air density
C_D	Aerodynamical drag coefficient
A_F	Frontal area of the vehicle
$\omega_{w,i}$	Angular velocity of the wheel i
F_i	Longitudinal force (friction force) acting at wheel i
Z_i	Vertical force acting at wheel i
$J_{w,i}$	Moment of inertia of wheel i
r	Wheel radius
μ_i	Friction coefficient of the road surface at wheel i
λ_i	Slip ratio of the wheel i
ε	Small positive number to prevent division by zero in (6)
B_i, C_i, D_i	Shape factors of the magic formula
$D_{s,i}$	Driving stiffness coefficient of the wheel i
G_i	Gear transformation ratio
$T_{wm,i}$	Wheel torque on the motor shaft i
$T_{mw,i}$	Motor torque on the wheel shaft i
$\omega_{m,i}$	Mechanical angular velocity of motor i
$T_{m,i}$	Torque of motor i
$J_{m,i}$	Moment of inertia of motor i
$P_{m,i}$	Output power of motor i
$P_{cu,i}, P_{fe,i}$	Copper loss and iron loss of motor i
$I_{d,i}, I_{q,i}$	The d- and q-axis armature currents of motor i
$I_{cd,i}, I_{cq,i}$	The d- and q-axis iron loss currents of motor i
$I_{od,i}, I_{oq,i}$	$I_{od,i} \triangleq I_{d,i} - I_{cd,i}, I_{cq,i} \triangleq I_{q,i} - I_{cq,i}$
$U_{d,i}, U_{q,i}$	The d- and q-axis terminal voltages of motor i
$L_{d,i}, L_{q,i}$	The d- and q-axis armature self-inductance
ρ_i	Salient coefficient of motor i: $\rho_i \triangleq L_{q,i}/L_{d,i}$
$R_{a,i}$	Armature winding resistance of motor i
$R_{c,i}$	Iron loss resistance of motor i
$\Psi_{e,i}$	Flux linkage of permanent magnet per-phase of motor i
$\Psi_{a,i}$	$\Psi_{a,i} \triangleq \sqrt{3}\Psi_{e,i}$
$\Psi_{eq,i}$	$\Psi_{eq,i} \triangleq \Psi_{a,i} + (1-\rho_i)L_{d,i}I_{od,i}$
$p_{n,i}$	Number of pole pairs of motor i
$\omega_{e,i}$	Electrical angular velocity of motor i

A. Longitudinal dynamics of EV

The N-wheel-EV is described in Fig. 1, in which $\boldsymbol{w}_i$ represents the general actuator mechanism, including the motor, gear, and wheel. We examine in Fig. 2 the motion of the $\boldsymbol{w}_i$. Assuming that the gear efficiency is 100%, the relationship between $\omega_{m,i}$ and $\omega_{w,i}$ is expressed as

$$\omega_{m,i} = G_i \omega_{w,i}, \quad T_{wm,i}\omega_{m,i} = T_{mw,i}\omega_{w,i} \tag{1}$$

The motions of the wheel and the motor are given by

$$J_{w,i}\dot{\omega}_{w,i} = T_{mw,i} - rF_i \tag{2}$$

$$J_{m,i}\dot{\omega}_{m,i} = T_{m,i} - T_{wm,i} \tag{3}$$

From (1), (2), (3), the equivalent motion of $\boldsymbol{w}_i$ is derived as

$$J_{eq,i}\dot{\omega}_{m,i} = T_{m,i} - G_i^{-1} rF_i \tag{4}$$

where the equivalent moment of inertia is

$$J_{eq,i} = J_{m,i} + G_i^{-2} J_{w,i} \tag{5}$$

The slip ratio of the wheel is defined as

$$\lambda_i = \frac{r\omega_{w,i} - v_x}{\max\left\{r\omega_{w,i}, v_x, \varepsilon\right\}} \tag{6}$$

In (6), $\max\left(r\omega_{w,i}, v_x, \varepsilon\right)$ is $r\omega_{w,i}$ in the driving mode, and v_x in the braking mode. The relationship between F_i and λ_i is commonly described by the magic formula [24]:

$$F_i = f_i(\lambda_i) = \mu_i Z_i \left\{B_i \tan^{-1}\left[C_i\lambda_i - D_i\left(C_i\lambda_i - \tan^{-1}\left(C_i\lambda_i\right)\right)\right]\right\} \tag{7}$$

If the slip ratio is small, the driving force can be linearized as

$$F_i \approx D_{s,i} Z_i \lambda_i \tag{8}$$

where $D_{s,i}$ can be identified from the experimental data [28].

To design the motion controllers, we can neglect the influences of the road slope and rolling resistance in the expression of the longitudinal motion of the vehicle body:

$$m\dot{v}_x = \sum_{i=1}^{N} F_i - \frac{1}{2}\sigma C_D A_F v_x |v_x| = \mathbf{1}_N^{\dagger}\mathbf{F} - \frac{1}{2}\sigma C_D A_F v_x |v_x| \tag{9}$$

where $\mathbf{1}_N = [1\ 1\ \ldots\ 1]^{\dagger}$ is the vector of size N, $\dagger$ is the transpose notation; and vector $\mathbf{F}$ consists of all F_i.

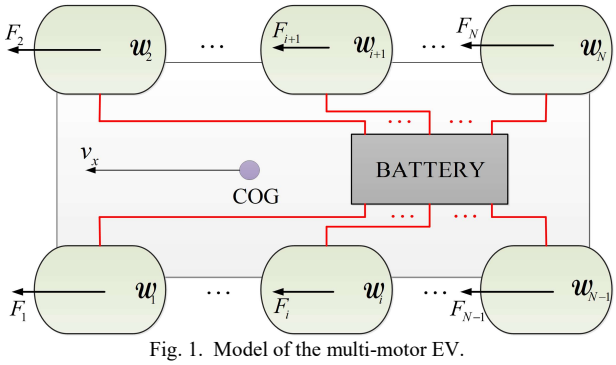

Fig. 1. Model of the multi-motor EV.

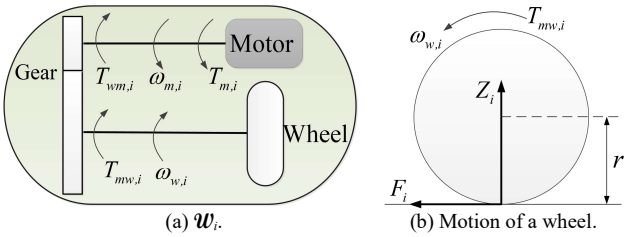

(a) $\boldsymbol{w}_i$. (b) Motion of a wheel.

Fig. 2. Model of the wheel-gear-motor mechanism.

B. Motor power model

As presented by Morimoto *et al.* in [25], we have

$$I_{cd,i} = -\frac{\omega_{e,i}\rho_i L_{d,i} I_{oq,i}}{R_{c,i}}, \quad I_{cq,i} = \frac{\omega_{e,i}\left(\Psi_{a,i} + L_{d,i} I_{od,i}\right)}{R_{c,i}} \tag{10a}$$

$$I_{od,i} = I_{d,i} - I_{cd,i}, \quad I_{oq,i} = I_{q,i} - I_{cq,i} \tag{10b}$$

$$T_{m,i} = p_{n,i}\Psi_{eq,i} I_{oq,i} \tag{10c}$$

$$\Psi_{eq,i} = \Psi_{a,i} + \left(1-\rho_i\right) L_{d,i} I_{od,i} \tag{10d}$$

$$\omega_{e,i} = p_{n,i}\omega_{m,i} \tag{10e}$$

$$P_{m,i} = \omega_{m,i} T_{m,i} \tag{11a}$$

$$P_{cu,i} = R_{a,i}\left(I_{d,i}^2 + I_{q,i}^2\right) \tag{11b}$$

$$P_{fe,i} = R_{c,i}\left(I_{cd,i}^2 + I_{cq,i}^2\right) \tag{11c}$$

In this study, the inverter loss and other losses are assumed to be uncontrollable. The minimization of motor input power is considered as the minimization of the summation of the input power $P_{m,i}$ with the copper loss $P_{cu,i}$ and iron loss $P_{fe,i}$ [18].

III. Passivity Approach

A. Introduction to passivity theory

We consider a system H with the state space equation

$$\begin{cases} \dot{x} = f(x,u) \\ y = g(x,u) \end{cases} \tag{12}$$

where the input and output vectors $u, y \in \mathrm{R}^p$, and the state vectors $x \in \mathrm{R}^n$.

Definition 1 [29]: The system H is passive from u to y if there exists a storage function $\mathrm{S}: \mathrm{R}^n \to \mathrm{R}_+$, such that

$\dot{S} \le y^{\dagger}u, \ \forall x \in \mathrm{R}^n, u \in \mathrm{R}^p$.

In addition, H is input strictly passive (ISP) if

$\dot{S} \le y^{\dagger}u - \delta_u\|u\|^2, \forall x \in \mathrm{R}^n, u \in \mathrm{R}^p$ for some $\delta_u > 0$,

and H is output strictly passive (OSP) if

$\dot{S} \le y^{\dagger}u - \delta_y\|y\|^2, \forall x \in \mathrm{R}^n, u \in \mathrm{R}^p$ for some $\delta_y > 0$.

The passivity notation is related to L_2-stability, which is a type of input-to-output stability. For instance, we examine in Fig. 3 the feedback connection of two subsystems H_1 and H_2.

Theorem 1 [29]: If both subsystems H_1 and H_2 are OSP, then system H with input (ξ_1, ξ_2) and output (y_1, y_2) has a finite L_2-gain. When $\xi_2 = 0$, the system H with input ξ_1 and output y_1 has a finite L_2-gain if either (i) H_1 is passive and H_2 is ISP, or (ii) H_1 is OSP and H_2 is passive.

B. Passivity analysis of EV longitudinal dynamics

We consider the EV as a system with the following input and output vectors, respectively:

$$\mathbf{T}_m = \begin{bmatrix} T_{m,1} & \ldots & T_{m,N} \end{bmatrix}^{\dagger}, \ \boldsymbol{\omega}_m = \begin{bmatrix} \omega_{m,1} & \ldots & \omega_{m,N} \end{bmatrix}^{\dagger}$$

Proposition 1: The EV is passive from $\mathbf{T}_m$ to $\boldsymbol{\omega}_m$.

Proof: We define the energy storage function as

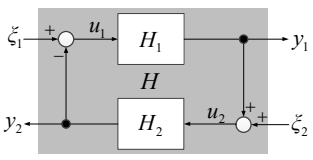

Fig. 3. Feedback connection of two subsystems.

$$S = S_V + \sum_{i=1}^{N} S_{W,i},\ S_V = \frac{1}{2} m v_x^2,\ S_{W,i} = \frac{1}{2} J_{eq,i} \omega_{m,i}^2 \tag{13}$$

From (1), (4), (9) and (13), we have:

$$\begin{aligned} \dot{S} - \boldsymbol{\omega}_m^{\dagger} \mathbf{T}_m &= m \dot{v}_x v_x + \sum_{i=1}^{N} J_{eq,i} \dot{\omega}_{m,i} \omega_{m,i} - \boldsymbol{\omega}_m^{\dagger} \mathbf{T}_m \\ &= \left(\mathbf{1}_N^{\dagger} \mathbf{F} - \frac{1}{2} \sigma C_D A_F v_x |v_x| \right) v_x + \sum_{i=1}^{N} \left(T_{m,i} - G_i^{-1} r F_i \right) \omega_{m,i} - \boldsymbol{\omega}_m^{\dagger} \mathbf{T}_m \\ &= -\frac{1}{2} \sigma C_D A_F v_x^2 |v_x| + \sum_{i=1}^{N} \left(F_i v_x - G_i^{-1} r F_i \omega_{m,i} \right) \\ &= -\frac{1}{2} \sigma C_D A_F v_x^2 |v_x| - \sum_{i=1}^{N} F_i \left(r \omega_{w,i} - v_x \right) \end{aligned} \tag{14}$$

In (14), the following term is always non-positive:

$$-\frac{1}{2} \sigma C_D A_F v_x^2 |v_x| \le 0 .$$

In the driving mode, we have $F_i \ge 0$ and $r\omega_{w,i} \ge v_x$. In the braking mode, we have $F_i \le 0$ and $r\omega_{w,i} \le v_x$. With respect to (6) and (7), the following term is also non-positive:

$$-F_i \left(r \omega_{w,i} - v_x \right) = -\max \left\{ r \omega_{w,i}, v_x, \varepsilon \right\} \lambda_i f(\lambda_i) .$$

Summarizing the two aforementioned terms, we recognize that the inequality $\dot{S} - \boldsymbol{\omega}_m^{\dagger} \mathbf{T}_m \le 0$ always hold true. This completes the proof.

Next, we will discuss the energy meaning of the storage function (13). We assume that the vehicle is in the driving mode. If the slip occurs, $\omega_{w,i}$, $\omega_{m,i}$ and its square $\omega_{m,i}^2$ will increase considerably. Consequently, much more energy will be consumed by the vehicle. Similarly, if the slip occurs in the braking mode, the vehicle will waste a huge amount of energy, which should be regenerated to the battery. In summary, the EMS should operate with the anti-slip capability to reduce the energy consumption of the vehicle.

IV. Double-layer EMS

A. Proposal of the double-layer configuration

The double-layer EMS is proposed in Fig. 4. The inner-layer includes an optimization algorithm (OP), which allocates the distribution ratios and the d-axis currents of the motors. In the outer-layer, the controller $C_w(s)$ is to control the aggregated speed ω_a to follow a reference pattern ω_r by generating the torque command T_{all}. Besides, the DOB is to improve the robustness of the control system under the change of road friction and model uncertainties [30]. The DOB includes a nominal model $P_n(s)$ and a low-pass filter $Q(s)$. The command T_a is the summation of T_{all} and the output T_d of the DOB. In Fig. 4 $\mathbf{k}$ is a nonzero distribution vector of size N, which consists of the distribution ratios $\{k_i\}$. Vector $\mathbf{T}_m$ is distributed from T_a, and $\boldsymbol{\omega}_m$ is aggregated to the scalar ω_a as follows:

$$\mathbf{T}_m = diag\left\{ G_i^{-1} \right\} \mathbf{k} T_a,\ \omega_a = \mathbf{k}^{\dagger} diag\left\{ G_i^{-1} \right\} \boldsymbol{\omega}_m \tag{15}$$

Proposition 2: In Fig. 4, the generalized vehicle model (GVM) with the input T_a and the output ω_a is passive.

Proof: From (15), the GVM is transparently passive:

$$\begin{aligned} \dot{S} - \omega_a^{\dagger} T_a &= \dot{S} - \left[\mathbf{k}^{\dagger} diag\left\{ G_i^{-1} \right\} \boldsymbol{\omega}_m \right]^{\dagger} T_a \\ &= \dot{S} - \boldsymbol{\omega}_m^{\dagger} diag\left\{ G_i^{-1} \right\} \left(\mathbf{k} T_a \right) = \dot{S} - \boldsymbol{\omega}_m^{\dagger} \mathbf{T}_m \le 0 \end{aligned}$$

B. Energy optimization problem

Thanks to the DOB based speed controller, it can be assumed that the slip ratio is maintained at a small value, or $v_x \approx r\omega_{w,i}$. From (6), we can approximate

$$\omega_{w,i} \approx \frac{v_x}{r} (1 + \lambda_i) \tag{16}$$

From (1) and (16), the motor speed can be expressed as

$$\omega_{m,i} \approx \frac{G_i v_x}{r} (1 + \lambda_i) \tag{17}$$

From (15), the motor torque is written as

$$T_{m,i} = \frac{k_i}{G_i} T_a \tag{18}$$

With respect to (4), the driving force is approximated as

$$F_i \approx \frac{G_i}{r} T_{m,i} \tag{19}$$

From (8), (18) and (19), the slip ratio is approximated as

$$\lambda_i \approx \frac{F_i}{D_{s,i} Z_i} \approx \frac{G_i T_{m,i}}{r D_{s,i} Z_i} \approx \frac{k_i T_a}{r D_{s,i} Z_i} \tag{20}$$

Under the assumption such that the slip ratio is small, we can approximate the electrical angular velocity as

$$\omega_{e,i} = p_{n,i} \omega_{m,i} \approx \frac{p_{n,i} G_i v_x}{r} \tag{21}$$

We substitute (17), (18) and (20) into (11a). Then, we substitute (10a) – (10e), (18) and (21) into (11b, c), the powers of the motor can be formulated as

$$P_{m,i} \approx \frac{v_x}{r} \left(1 + \frac{k_i T_a}{r D_{s,i} Z_i} \right) k_i T_a \tag{22a}$$

$$P_{cu,i} = R_{a,i} \left\{ \begin{aligned} &\left(I_{od,i} - \frac{v_x \rho_i L_{d,i}}{r R_{c,i}} \frac{k_i T_a}{\Psi_{eq,i}} \right)^2 \\ &+ \left[\frac{1}{p_{n,i} \Psi_{eq,i}} \cdot \frac{k_i T_a}{G_i} + \frac{p_{n,i} G_i v_x \left(\Psi_{a,i} + L_{d,i} I_{od,i} \right)}{r R_{c,i}} \right]^2 \end{aligned} \right\} \tag{22b}$$

$$P_{fe,i} = \frac{p_{n,i}^2 G_i^2 v_x^2}{r^2 R_{c,i}} \left\{ \frac{\rho_i^2 L_{d,i}^2 k_i^2 T_a^2}{p_{n,i}^2 \Psi_{eq,i}^2 G_i^2} + \left(\Psi_{a,i} + L_{d,i} I_{od,i} \right)^2 \right\} \tag{22c}$$

We consider the following optimization problem:

$$\begin{aligned} &\min_{\{k_i, I_{od,i}\}} \sum_{i=1}^{N} \left(P_{m,i} + P_{cu,i} + P_{fe,i} \right) \\ &\text{s.t.} \sum_{i=1}^{N} k_i = 1,\ 0 \le k_i \le 1 \end{aligned} \tag{23}$$

Problem (23) can be solved using a Lagrange multiplier algorithm. To perform the algorithm, Z_i can be calculated in real-time using on-board sensors [31]. From (4), the driving force observer can be designed to estimate F_i by using $T_{m,i}$ and $\omega_{m,i}$ [18]. To identify $D_{s,i}$ using the linearized relationship (8), the slip ratio could be firstly estimated [32].

C. General design procedure

The equivalent block diagram of the double-layer EMS is described in Fig. 5, where the equivalent transfer functions are

$$C_{eql}(s) = \frac{F(s) Q(s)}{P_n(s)},\ C_{equ}(s) = F(s) C_w(s),\ F(s) = \frac{1}{1 - Q(s)} \tag{24}$$

Design procedure of the double-layer EMS

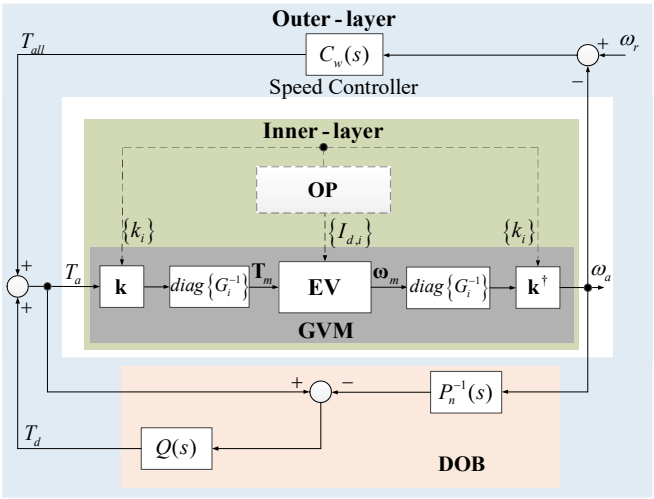

Fig. 4. Block diagram of the proposed double-layer EMS.

Stage 1-Inner-layer: Design the algorithm to solve the optimization problem (23).

Stage 2-Outer-layer: Select the transfer functions $P_n(s)$, $Q(s)$, and $C_w(s)$ such that: $F(s)$ is stable; $C_{eql}(s)$ is passive; $C_w(s)$ and $C_{equ}(s)$ are OSP.

Proposition 3: The above design procedure sufficiently guarantees that the equivalent system in Fig. 5 (with input ω_r and output T_{equ}) has a finite L_2-gain.

Proof: The stability of $F(s)$ is to ensure internal stability of the signals. The system $\mathcal{L}$ in the red dashed rectangle of Fig. 5 is the feedback connection of GVM and C_{eql}. From Proposition 2, GVM is passive. Thus, if C_{eql} is designed to be passive, then it can be shown from Definition 1 that $\mathcal{L}$ is also passive. The overall system in Fig. 5 is the feedback connection of $\mathcal{L}$ and C_{equ}. Following Theorem 1, if C_{equ} is OSP, then the overall system in Fig. 5 is also OSP and has a finite L_2-gain.

D. Remarks on the implementation of double-layer EMS

Remark 1: The current constraint can be included in the OP (23) without any change in the configuration of the double-layer EMS in Fig. 4. From literature review, there are several studies that considered the motor loss reduction with respect to the saturation of the currents [33], [34]. However, this issue is not the main goal of this paper. In this study, we focus on the EMS configuration that can integrate energy optimization and safe longitudinal motion control, and find a strategy to stabilize the overall system in a practical way.

Remark 2: If the gear efficiency η_i should be addressed, the system EV is passive from $\mathbf{T}_m$ to $\tilde{\boldsymbol{\omega}}_m = diag\{\eta_i\}\boldsymbol{\omega}_m$ with the storage function $\tilde{S} = S_V + \sum_{i=1}^{N}\eta_i S_{W,i}$ and $\tilde{J}_{eq,i} = J_{m,i} + \eta_i G_i^{-2} J_{w,i}$. Therefore, the proposed double-layer EMS is still applicable.

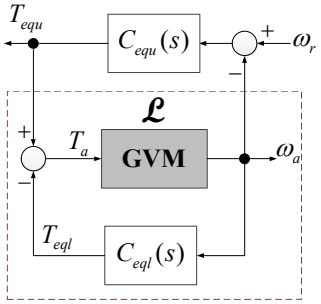

Fig. 5. Equivalent block diagram of the proposed double-layer EMS.

V. Design Example

A. Three-wheel EV model

To demonstrate the effectiveness of the double-layer EMS, this study used the 3-wheel-EV model ($N = 3$). This model has been used as a workbench for our research in [23] and [35]. The vehicle is now driven by a 13 kW PMSM connected to the rear wheel through 2 pulleys and belt. Two 4kW axial PMSMs are directly connected to the front wheels. The main physical parameters and the photo of the vehicle under study are listed in TABLE A1 of the Appendix.

B. Design of the inner-layer

Substitute (10d) into (22b), the copper-loss can be derived as in (25), which is expressed at the top of the following page. Summarizing (22a), (22c) and (25), we obtain

$$\sum_{i=1}^{3}\left(P_{m,i} + P_{cu,i} + P_{fe,i}\right) = P^{\mathcal{K}} + \sum_{i=1}^{3} P_i^{\mathcal{J}} \tag{26a}$$

$$P^{\mathcal{K}} = \sum_{i=1}^{3} P_i^{\mathcal{K}} \tag{26b}$$

$$P_i^{\mathcal{K}} = \alpha_i\left(k_i T_a\right)^2 + \frac{v_x}{r}\left(1 + \frac{2R_{a,i}}{R_{c,i}}\right)k_i T_a \tag{26c}$$

$$\alpha_i = R_{a,i}\left[\left(\frac{v_x \rho_i L_{d,i}}{rR_{c,i}\Psi_{eq,i}}\right)^2 + \left(\frac{1}{G_i p_{n,i}\Psi_{eq,i}}\right)^2\right] + \frac{v_x^2 \rho_i^2 L_{d,i}^2}{r^2 R_{c,i}\Psi_{eq,i}^2} + \frac{v_x}{r^2 D_{s,i} Z_i} \tag{26d}$$

$$P_i^{\mathcal{J}} = \beta_i I_{od,i}^2 + \gamma_i I_{od,i} + \left(R_{a,i} + R_{c,i}\right)\left(\frac{p_{n,i} G_i v_x}{rR_{c,i}}\right)^2 \Psi_{a,i}^2 \tag{26e}$$

$$\beta_i = R_{a,i} + \left(R_{a,i} + R_{c,i}\right)\left(\frac{p_{n,i} G_i v_x}{rR_{c,i}}\right)^2 L_{d,i}^2 \tag{26f}$$

$$\gamma_i = 2\left(R_{a,i} + R_{c,i}\right)\left(\frac{p_{n,i} G_i v_x}{rR_{c,i}}\right)^2 \Psi_{a,i} L_{d,i} \tag{26g}$$

From a practical point of view, we notice that:

First, in almost PMSMs, the armature winding resistance $R_{a,i}$ is significantly small in comparison with the iron loss resistance $R_{c,i}$. In case of the 3-wheel EV under study, $2R_{a,i}/R_{c,i}$ is less than 0.1% for both the front wheel motors ($i = 1, 2$) and rear wheel motor ($i = 3$).

Second, by calculation using the motor parameters in TABLE A1, it can be observed that the value of $\Psi_{eq,i}$ is quite close to $\Psi_{a,i}$. Even when $I_{od,i}$ reached the amplitude of -40[A], $\Psi_{eq,i}$ only deviates 0.64% from $\Psi_{a,i}$ for the front wheel motors. This deviation is about 1.33% for the rear wheel motor.

Thus, it is reasonable to approximate:

$$P_i^{\mathcal{K}} \approx \tilde{P}_i^{\mathcal{K}} = \tilde{\alpha}_i\left(k_i T_a\right)^2 + \frac{v_x}{r} k_i T_a \tag{27}$$

$$P_{cu,i} = R_{a,i} I_{od,i}^2 + R_{a,i}\left(\frac{v_x \rho_i L_{d,i}}{r R_{c,i} \Psi_{eq,i}}\right)^2 (k_i T_a)^2 + R_{a,i}\left(\frac{1}{G_i p_{n,i} \Psi_{eq,i}}\right)^2 (k_i T_a)^2 + \left(\frac{p_{n,i} G_i v_x}{r R_{c,i}}\right)^2 \left(\Psi_{a,i} + L_{d,i} I_{od,i}\right)^2$$
$$+ 2R_{a,i} \frac{v_x}{r R_{c,i} \Psi_{eq,i}} \left[\Psi_{a,i} + (1-\rho_i) L_{d,i} I_{od,i}\right] k_i T_a \tag{25}$$
$$= R_{a,i} I_{od,i}^2 + R_{a,i}\left(\frac{v_x \rho_i L_{d,i}}{r R_{c,i} \Psi_{eq,i}}\right)^2 (k_i T_a)^2 + R_{a,i}\left(\frac{1}{G_i p_{n,i} \Psi_{eq,i}}\right)^2 (k_i T_a)^2 + \left(\frac{p_{n,i} G_i v_x}{r R_{c,i}}\right)^2 \left(\Psi_{a,i} + L_{d,i} I_{od,i}\right)^2 + 2R_{a,i} \frac{v_x}{r R_{c,i}} k_i T_a$$

$$\tilde{\alpha}_i = R_{a,i}\left[\left(\frac{v_x \rho_i L_{d,i}}{r R_{c,i} \Psi_{a,i}}\right)^2 + \left(\frac{1}{G_i p_{n,i} \Psi_{a,i}}\right)^2\right] + \frac{v_x^2 \rho_i^2 L_{d,i}^2}{r^2 R_{c,i} \Psi_{a,i}^2} + \frac{v_x}{r^2 D_{s,i} Z_i} \tag{28}$$

The OP (23) with $N = 3$ can be approximately solved by:

$$\min_{\{k_i, I_{od,i}\}} \left(\tilde{P}^{\mathcal{K}} + \sum_{i=1}^{3} P_i^{\mathcal{J}}\right) \quad \text{s.t.} \sum_{i=1}^{3} k_i = 1,\ 0 \le k_i \le 1 \tag{29}$$

Each $P_i^{\mathcal{J}}$ is a quadratic function of only $I_{od,i}$. Besides, $\tilde{P}^{\mathcal{K}}$ is a summation of three functions $\tilde{P}_i^{\mathcal{K}}$, each of which is a quadratic function of k_i. Therefore, the problem (29) can be solved via the following algorithm.

Practical algorithm for energy optimization

Step-1: Using the measured/estimated values of v_x, $D_{s,i}$, Z_i to update $\tilde{\alpha}_i$, β_i, γ_i by the formula (28), (26f) and (26g).

Step-2: Solve $\partial P_i^{\mathcal{J}} / \partial I_{od,i} = 0$ to obtain the optimal current

$$I_{od,i}^* = -\frac{\gamma_i}{2\beta_i}.$$

Step-3: Solve $\min_{\{k_i\}} \tilde{P}^{\mathcal{K}}$ s.t.: $\sum_{i=1}^{3} k_i = 1, 0 \le k_i \le 1$, to obtain

$$k_i^* = \frac{\tilde{\alpha}_i^{-1}}{\sum_{i=1}^{3} \tilde{\alpha}_i^{-1}}.$$

Step-4: Based on the equivalent circuit of the PMSM, the motor currents are calculated as

$$I_{d,i}^* = I_{od,i}^* - \frac{v_x}{r} \frac{\rho_i L_{d,i}}{R_{C,i}} \frac{k_i^* T_a}{\left[\Psi_{a,i} + (1-\rho_i) L_{d,i} I_{od,i}^*\right]},$$

$$I_{q,i}^* = \frac{k_i^* T_a}{p_{n,i} G_i \left[\Psi_{a,i} + (1-\rho_i) L_{d,i} I_{od,i}^*\right]} + \frac{p_{n,i} G_i v_x \left(\Psi_{a,i} + L_{d,i} I_{od,i}^*\right)}{r R_{C,i}}.$$

Thanks to the above analytical expressions, the proposed algorithm can be implemented conveniently in either simulation or experiment. Given a speed v_x, we can instantaneously determine the optimal distribution ratios and flux currents. Note that, v_x can be obtained via slip ratio estimation [32]. We neglect to present the slip ratio estimation, which is not the goal of this paper.

C. Design of the outer-layer

We select the DOB with a first order nominal model, a first order low-pass filter; and the speed controller is chosen as a first order compensator:

$$P_n(s) = \frac{1}{J_n s},\ Q(s) = \frac{K_f}{\tau_f s + 1},\ C_w(s) = K_w \frac{\tau_f s + 1 - K_f}{\tau_w s + 1} \tag{30}$$

where J_n is the parameter of the nominal model, τ_f is the time constant of the low-pass filter, and K_f is a tuning parameter.

Substitute (30) into (24), we have

$$C_{eql}(s) = \frac{K_f J_n s}{\tau_f s + 1 - K_f}, C_{equ}(s) = K_w \frac{\tau_f s + 1}{\tau_w s + 1}, F(s) = \frac{\tau_f s + 1}{\tau_f s + 1 - K_f} \tag{31}$$

Proposition 4: Select the nominal inertia $J_n > 0$, the time constants $\tau_f > 0$ and $\tau_w > 0$, the DOB gain $K_f \in (0, 1)$, and the speed control gain $K_w > 0$ such that

$$\begin{bmatrix} -2\phi_1 \frac{1}{\tau_w} + 2\delta_1 K_w^2 & \phi_1 b_1 - K_w + 2\delta_1 K_w^2 \\ \phi_1 b_1 - K_w + 2\delta_1 K_w^2 & -2K_w + 2\delta_1 K_w^2 \end{bmatrix} \le 0 \tag{32a}$$

$$\begin{bmatrix} -2\phi_2 \frac{1}{\tau_w} + 2\delta_2 K_w^2 & \phi_2 b_2 - K_w + 2\delta_2 K_w^2 \\ \phi_2 b_2 - K_w + 2\delta_2 K_w^2 & -2K_w + 2\delta_2 K_w^2 \end{bmatrix} \le 0 \tag{32b}$$

for some non-negative numbers $\phi_{1,2}$ and some positive numbers $\delta_{1,2}$, with

$$b_1 = \frac{1 - K_f}{\tau_f} - \frac{1}{\tau_w},\ b_2 = \frac{1}{\tau_f} - \frac{1}{\tau_w} \tag{32c}$$

then the selection (30) of the outer-layer satisfies the general design procedure of double-layer EMS.

Proof: It is clear that if $\tau_f > 0$ and $K_f \in (0, 1)$ then the transfer function $F(s)$ is stable. If J_n and τ_w are also positive, then C_{eql} can be represented in Fig. 6 as a feedback connection of two passive systems. Hence, C_{eql} is also passive. Finally, the conditions (32a, b) are obtained by applying the Kalman − Yakubovich − Popov (KYP) Lemma [36] to the state space representations of C_w and C_{eql}.

VI. Evaluation Test and Discussion

A. Preparation for the evaluation

Using the physical parameters in TABLE A1, a simulator of the 3-wheel-EV was established using Matlab/Simulink. This simulator was used for the evaluation test in our study [23]. To imitate the actual vehicle's behavior, the simulator includes the

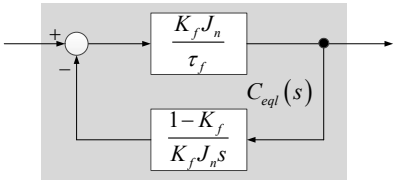

Fig. 6. Representation of C_{eql} as a feedback connection of two systems.

nonlinear tire force models based on the magic formula. It also includes motor drive models and battery models. The control period of the simulator was set to be 1ms, which is similar to the experimental system. Using the simulator and Proposition 4, we conducted a fine-tuning process to select the gains of the DOB and the compensator, which are expressed in (30). A set of control parameters that attained good motion control performance was chosen as: $\{J_n = 34, K_f = 0.8, \tau_f = 0.05, K_w = 2500, \tau_w = 0.15\}$.

B. Test 1: Critical driving test

As listed in TABLE III, four EMS methods were performed. For a fair comparison, the four methods used the same speed controller $C_w(s)$. The longitudinal speed pattern of this test is shown in Fig. 7(a). The reference ω_r is calculated by dividing the speed pattern by the wheel radius r. As shown in Fig. 7(b), the road friction coefficient reduces from the high value of 0.807 to the low value of 0.250 three times.

The speed responses of the four methods are shown in Figs. 7(c) - 7(f). Due to the symmetry, the speeds of the front-left and front-right wheels are almost the same. For the sake of clarity, we will not demonstrate the speed of the front-right wheel in these figures. Method-1 and Method-2 experienced serious wheel slip when accelerating on the low friction surface. Using Method-2, the vehicle mainly suffered the slip at the front wheels (see Fig. 7(d)). Using Method 1, which allocates more torque to the rear wheel to satisfy its energy optimization algorithm, the vehicle mainly suffered the slip at the rear wheel (see Fig. 7(c)). In contrast, Method-3 and Method-4 can considerably suppress the wheel slip. As shown in Fig. 7(e) and Fig. 7(f), the longitudinal speeds of the wheels are always close to those of the vehicle body. For better evaluation of the anti-slip performance, we define the average slip ratio index as follows:

$$\bar{\lambda} = \frac{\lambda_1 + \lambda_2 + \lambda_3}{3} \tag{33}$$

Fig. 8 demonstrates the average slip ratio in the driving period from 65.8 to 69.8[s]. In this period, the vehicle has to accelerate at 3 [m/s^2] while experiencing a sharp change in road friction. The average slip ratios of Method-1 and Method-2 are always larger than those of Method-3 and Method-4. Although Method-4 is quite simple in its configuration, its anti-slip performance is almost close to that of Method-3.

The energy consumptions of the four methods are compared in Fig. 9(a). Using Method-1, the vehicle must consume much more energy (285.6 Wh). Method-2 still lacks the slip prevention, and the vehicle must consume 139 Wh . By preventing the wheel slip, the energy consumption of the vehicle with Method-3 was only 96.96 Wh. Method-4 is the best in term of energy savings. Using this method, the vehicle can prevent the wheel slip and simultaneously optimize the torque distribution and flux-currents. It only consumes an energy of 86.43 Wh. The distribution ratios and flux-currents of Method-4 are shown in Figs. 9(b) and (c), respectively.

C. Test 2: New European Driving Cycle (NEDC) test

This paper utilizes the NEDC to analyze the performance of the double-layer EMS with different torque and flux-current distribution strategies. The NEDC's speed pattern and the change of road friction are shown in Figs. 10(a) and (b), respectively. During the NEDC, there are four periods in which the road friction changes from a high value to an exceptionally low value. The four distribution strategies are summarized in TABLE IV. The strategy S#-A (# = {1, 2, 4}) maintains the motor flux current at zero value. The strategy S#-B (# = {1, 2, 4}) optimizes the motor flux current by the method proposed by Morimoto *et al.* [25]. The strategy S3 utilizes the practical algorithm presented in the previous Section.

TABLE III
DESCRIPTION OF THE EVALUATED METHODS IN TEST 1

No.	Scheme			
	Speed control	Energy optimization		Reference
		Torque	Flux current	
1	The longitudinal speed of the vehicle is control by the controller C_w(s) but the DOB is not utilized.	The torque distribution ratios are updated to minimize the motor input power.	The motor flux currents are maintained at zero.	The torque distribution algorithm was developed by Fujimoto and Harada [17].
2	The longitudinal speed of the vehicle is control by the controller C_w(s) but the DOB is not utilized.	The torques are equally distributed: $k_i = 1/3\ \forall i \in \{1,2,3\}$.	The motor flux currents are updated to minimize the copper and iron losses.	The loss minimization algorithm was presented in the work of Morimoto *et al.* on PMSM control [25].
3	The aggregated wheel speed is control by the controller C_w(s) and each wheel is provided a DOB.	The torque distribution ratios are updated to minimize the motor input power.	The motor flux currents are maintained at zero.	The system design condition and the optimization algorithm were presented in our recent study [23].
4	The speed controller C_w(s) and a unique DOB is applied to the generalized vehicle model.	The torque distribution ratios and the motor flux currents are *simultaneously updated* to minimize the motor input power.		The double-layer EMS *proposed* in this paper with the OP (23) and the practical algorithm in Section V.

TABLE IV
DESCRIPTION OF THE TORQUE & FLUX-CURRENT DISTRIBUTION STRATEGIES EVALUATED IN TEST 2

Strategy S1 Almost front drive		**Strategy S2** Equal torque distribution		**Strategy S3** The proposed OP (23)	**Strategy S4** Almost rear drive	
S1-A	S1-B	S2-A	S2-B	$\{k_i, I_{d,i}\}$ is obtained by the OP (23) with the practical algorithm in Section V.	S4-A	S4-B
$k_{1,2} = 0.45$ $k_3 = 0.05$ $I_{d,i} = 0$	$k_{1,2} = 0.45$ $k_3 = 0.05$ $I_{d,i} = opt$	$k_{1,2} = 1/3$ $k_3 = 1/3$ $I_{d,i} = 0$	$k_{1,2} = 1/3$ $k_3 = 1/3$ $I_{d,i} = opt$		$k_{1,2} = 0.05$ $k_3 = 0.90$ $I_{d,i} = 0$	$k_{1,2} = 0.05$ $k_3 = 0.90$ $I_{d,i} = opt$

This article has been accepted for publication in IEEE Transactions on Vehicular Technology. This is the author's version which has not been fully edited and content may change prior to final publication. Citation information: DOI 10.1109/TVT.2023.3244808

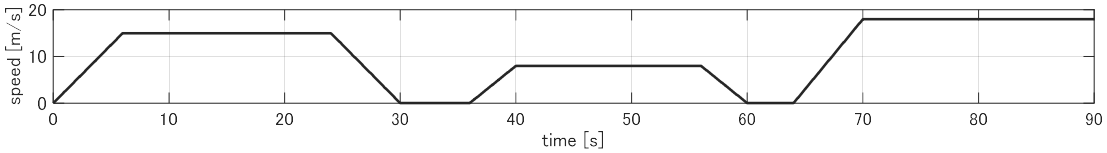

(a) Speed pattern.

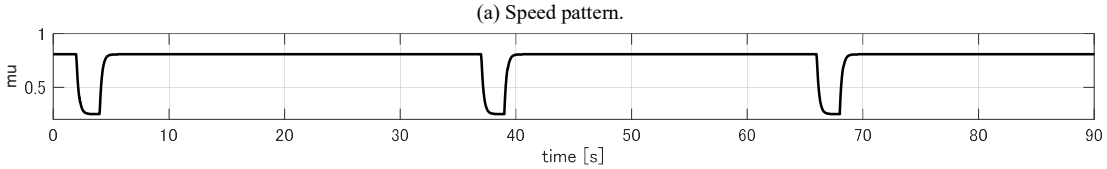

(b) Change of road friction coefficient.

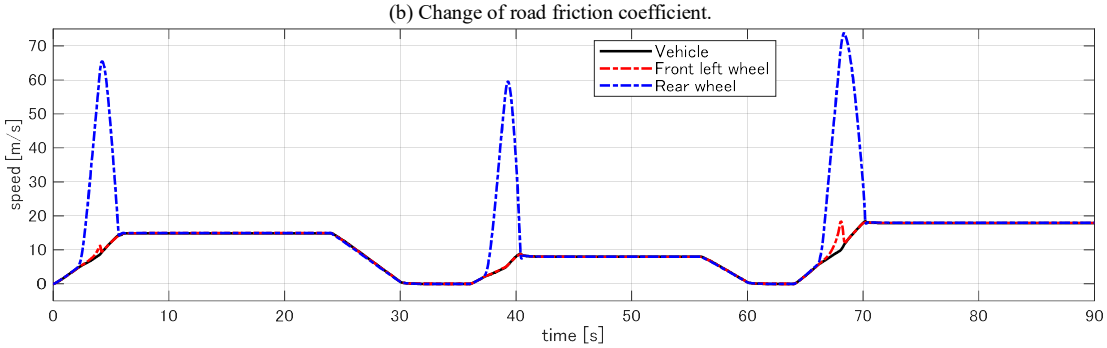

(c) Method-1.

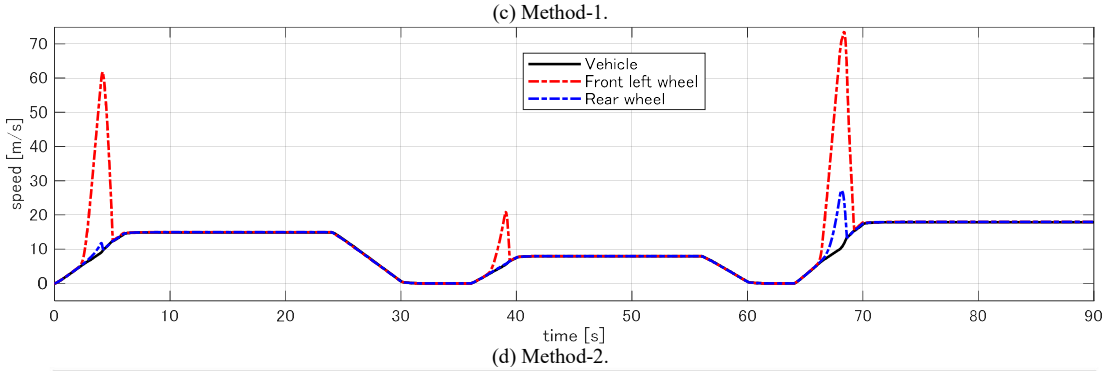

(d) Method-2.

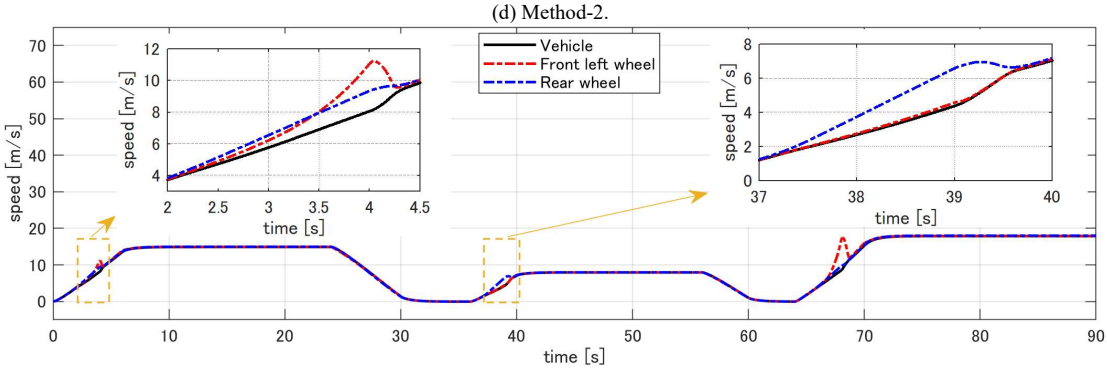

(e) Method-3.

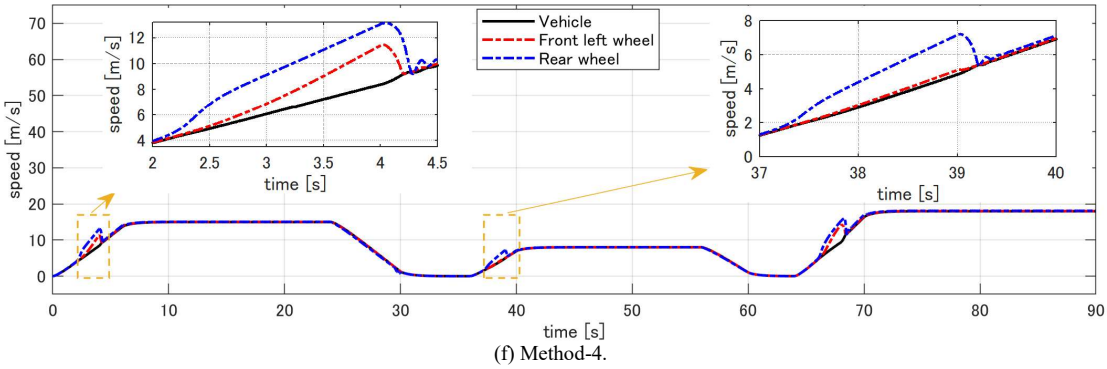

(f) Method-4.

Fig. 7. **Test 1**: Longitudinal speeds of the vehicle body and the wheels.

This article has been accepted for publication in IEEE Transactions on Vehicular Technology. This is the author's version which has not been fully edited and content may change prior to final publication. Citation information: DOI 10.1109/TVT.2023.3244808

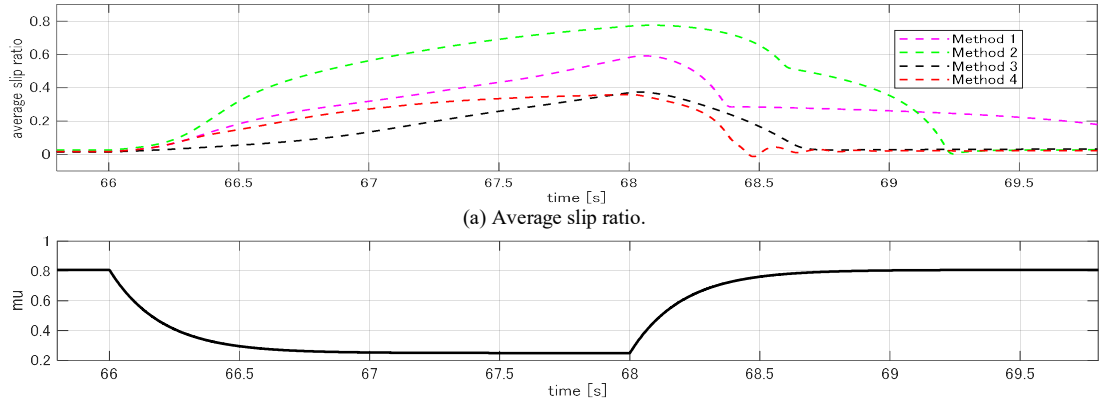

(a) Average slip ratio.

(b) Change of road friction coefficient.

Fig. 8. **Test 1**: Average slip ratio of four methods between 65.8 and 69.8[s].

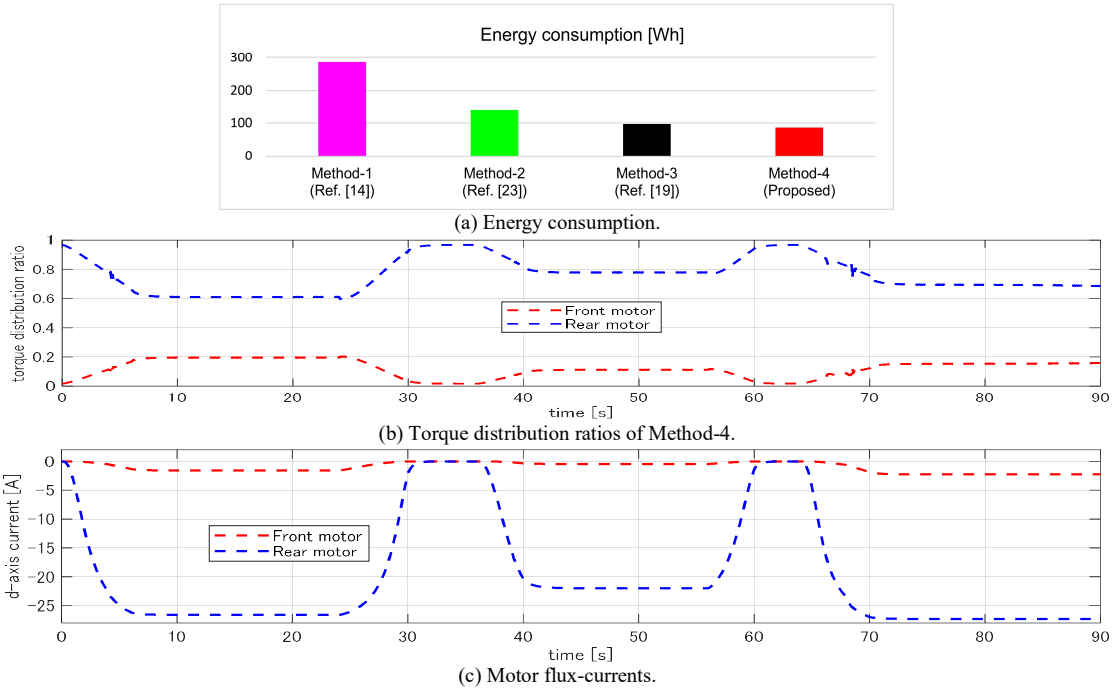

(a) Energy consumption.

(b) Torque distribution ratios of Method-4.

(c) Motor flux-currents.

Fig. 9. **Test 1**: Comparison of energy consumption.

The energy consumptions of the strategies in TABLE IV are shown in Fig. 11(a). By maintaining zero flux-currents, the energy consumptions of the vehicle with S1-A, S2-A, and S4-A are 1193 Wh, 1165 Wh, and 1186 Wh, respectively. By updating the flux-currents to minimize the power loss, the energy consumption of the vehicle with S1-B, S2-B, and S3-B are 1018 Wh, 987.3 Wh, and 996.9 Wh, respectively. By simultaneously distributing the torques and flux-currents to minimize the input power, S3 is the best in term of energy consumption. Utilizing S3, the vehicle consumed only 969.6 Wh. In comparison with the worst strategy of S1-A, energy consumption is reduced 18.7% by S3.

The battery state of charges (SOCs) in accordance with the aforementioned strategies are illustrated in Fig. 11(b). Transparently, the SOC curves of S1-A, S2-A and S3-A are always in the lower positions in comparison with the SOC curves of S1-B, S2-B, and S4-B. Until the end of the NEDC, the SOC curve of S3 always dominates the highest position. These results prove the effectiveness of OP (23). The optimal values of the distribution ratios and flux-currents obtained by S3 are shown in Fig. 12(a) and Fig. 12(b), respectively.

VII. Conclusion

This paper proposes a double-layer EMS, which can effectively utilize the electric energy by preventing the wheel slip and optimally distributing both the torque commands and the flux currents of the motors. Although the vehicle dynamics is quite complex, L_2 stability of the proposed EMS can be shown rigorously without any complex mathematic calculation. Also, the passivity-based design strategy used in this paper can be applied to the other complex systems. Energy management and safe traction can be attained simultaneously by a simple design procedure. In addition, the analytical solution of the energy optimization allows double-layer EMS to be implemented quickly and conveniently. The effectiveness of the proposed system has been verified by two test scenarios

This article has been accepted for publication in IEEE Transactions on Vehicular Technology. This is the author's version which has not been fully edited and content may change prior to final publication. Citation information: DOI 10.1109/TVT.2023.3244808

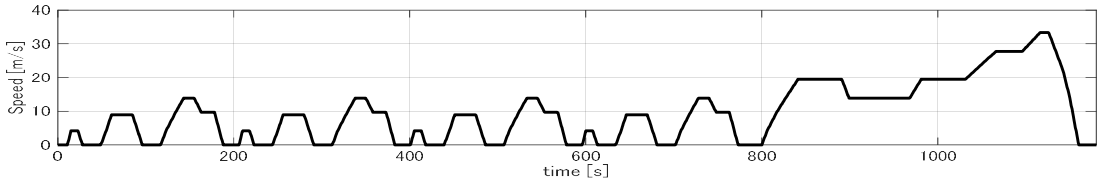

(a) Speed pattern.

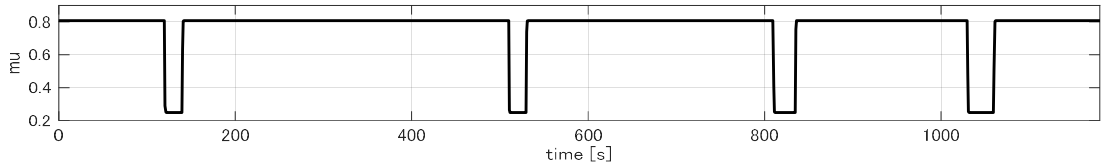

(b) Change of road friction coefficient.

Fig. 10. **Test 2**: Setting of the New European Driving Cycle test.

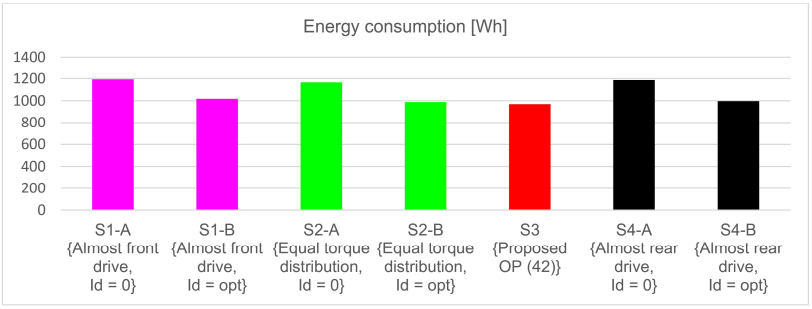

(a) Energy consumption.

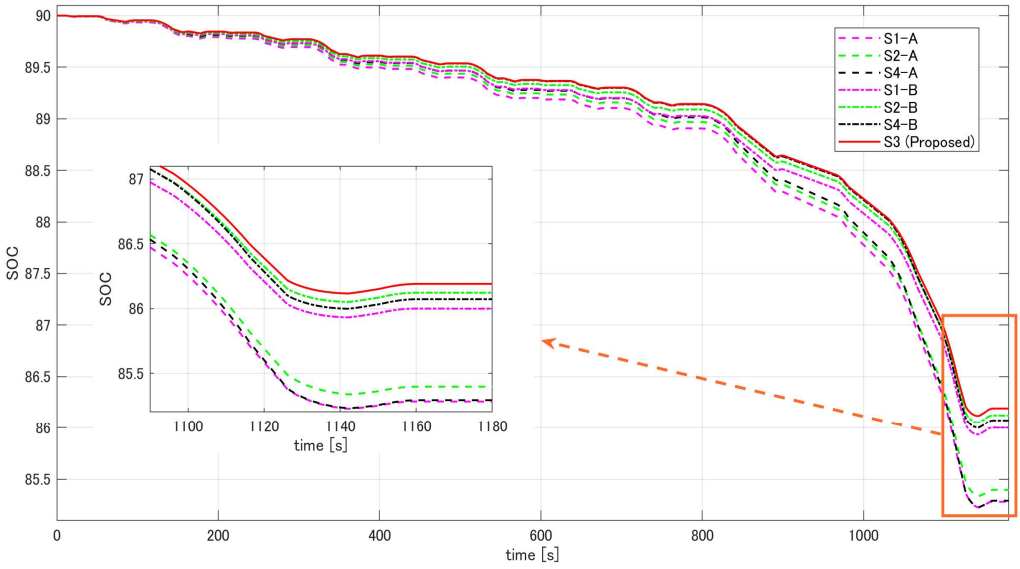

(b) Battery state of charge.

Fig. 11. **Test 2**: Comparison of different torque and flux-current distribution strategies.

using a three-wheel EV model. The double-layer EMS can straightforwardly be extended to other EV prototypes, such as in-wheel-motor EVs.

In the future, we will examine the EMS for considering both motor side and source side. We will also investigate the higher order speed controller and the optimization of the control parameters to improve the performance of speed tracking control in the outer-layer. With respect to the nonlinearity and complexity of the multi-motor EV system, data-driven, fuzzy logic and intelligent control algorithms can also be considered in the double-layer EMS framework.

APPENDIX

The physical parameters of the 3-wheel EV used for evaluation are summarized in TABLE A1.

Considering the longitudinal dynamics of the three-wheel EV, we have:

$$Z_{1,2} = \frac{ml_r}{2(l_f + l_r)} g - \frac{mh_g}{2(l_f + l_r)} \frac{dv_x}{dt} \tag{a1}$$

$$Z_3 = \frac{ml_f}{(l_f + l_r)} g + \frac{mh_g}{(l_f + l_r)} \frac{dv_x}{dt} \tag{a2}$$

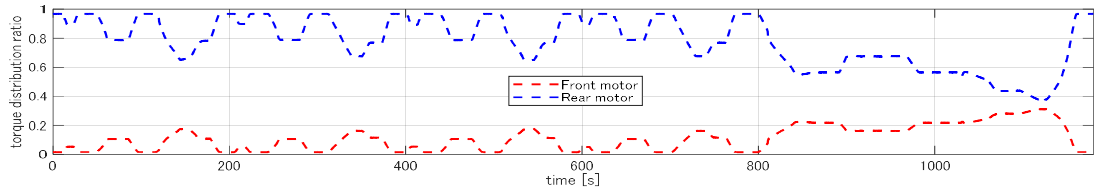

(a) Torque distribution ratios.

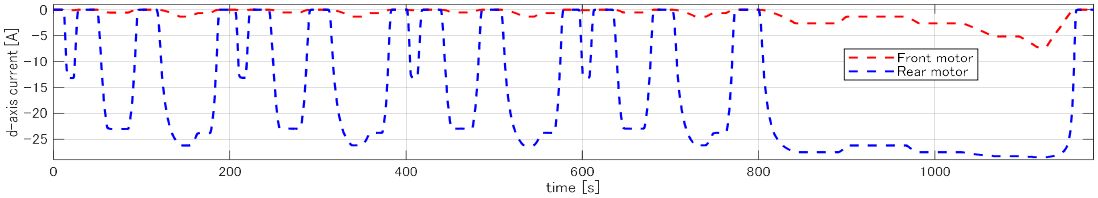

(b) Motor flux-currents.

Fig. 12. **Test 2**: Optimal torque distribution ratios and motor flux-currents given by strategy S3 .

From (28), (a1) and (a2), the optimal torque distribution ratios rely on the driving stiffness $D_{s,i}$ and the position of the COG. Such equations can be used to analyze the sensitivity of the proposed EMS to the variations of $\{D_{s,i}, l_f, l_r, h_g\}$.

TABLE A1
PHYSICAL PARAMETERS OF THE 3-WHEEL-EV

Vehicle mass (without driver)	$m = 350$ kg
Wheel's radius	$r = 0.27$ m
Gear transformation ratio	$G_1 = G_2 = 1.0, G_3 = 5.033$
Inertia of the wheel	$J_{w,1} = J_{w,2} = 0.6847$ kg. m^2 $J_{w,3} = 1.055$ kgm^2
Inertia of the motor shaft	$J_{m,1} = J_{m,2} = 0.060$ kg. m^2 $J_{m,3} = 0.096$ kg. m^2
Distance from center of gravity to front and rear axles	$L_f = 0.678$ m $L_r = 1.039$ m
Height of center of gravity	$H_g = 0.65$ m
Frontal area of the vehicle	$A_F = 1.25$ m^2
Rear motor	$R_{c,3} = 300.13\ \Omega$ $R_{a,3} = 0.082\ \Omega$ $L_{d,3} = 0.00062$ H $L_{q,3} = 0.00068$ H $\Psi_{a,3} = 0.181$ Wb $p_{n,3} = 10$
Front motor	$R_{c,1(2)} = 300.15\ \Omega$ $R_{a,1(2)} = 0.142\ \Omega$ $L_{d,1(2)} = 0.0013$ H $L_{q,1(2)} = 0.0015$ H $\Psi_{a,1(2)} = 0.126$ Wb $p_{n,1(2)} = 12$

Photo of the vehicle under study.

REFERENCES

[1] Y. Hori, "Future Vehicle Driven by Electricity and Control-Research on 4 Wheel Motored UOT Mach II," IEEE Transactions on Industrial Electronics, Vol. 51, No. 5, pp. 954-962, 2004.

[2] J. Brembeck, R. De Castro, J. Tobolar, and I. Ebrahimi, "IEEE VTS Motor Vehicles Challenge 2023: A Multi-physical Benchmark Problem for Next Generation Energy Management Algorithms," 19th IEEE Vehicle Power and Propulsion Conference (VPPC), 2022.

[3] H. Khayyam, A.Z. Kouzani, S. Nahavandi, V. Marano, G. Rizzoni, "Intelligent Energy Management in Hybrid Electric Vehicles," Energy Management, Francisco Maciá Pérez (ed), Vienna, Austria (2010), pp. 147–175, ISBN 978-953-307-065-0, IN-TECH.

[4] M. Abe, "Trends of Intelligent Vehicle Dynamics Controls and Their Future," NTN Technical Review, No. 81, pp. 2-11, 2013.

[5] Y. Suzuki, Y. Kano, and M. Abe, "A study on Tyre Force Distribution Controls for Full Drive-by-wire Electric Vehicle," Vehicle System Dynamics, Vol. 52, pp. 235-250, 2014.

[6] B. Zhao, N. Xu, H. Chen, K. Guo, and Y. Huang, "Design and Experimental Evaluations on Energy-Efficient Control for 4WIMD-EVs Considering Tire Slip Energy," IEEE Transactions on Vehicular Technology, Vol. 69, No. 12, pp. 14631-14644, 2020.

[7] P. He and Y. Hori, "Improvement of EV Maneuverability and Safety by Dynamic Force Distribution with Disturbance Observer," World Electric Vehicle Journal, Vol. 1, No. 1, pp. 258-263, 2007.

[8] O. Mokhiamar and M. Abe, "How the Four Wheels Should Share Forces in an Optimum Cooperative Chassis Control," Control Engineering Practice, Vol. 14, Iss. 3, pp. 295-304, 2006.

[9] B. Leng, L. Xiong, Z. Yu, and T. Zou, "Allocation Control Algorithms Design and Comparison Based on Distributed Drive Electric Vehicles," International Journal of Automotive Technology, Vol. 19, No. 1, pp. 55-62, 2018.

[10] L. De Novellis, A. Sorniotti, P. Gruber, L. Shead, V. Ivanov, and K. Hoepping, "Torque Vectoring for Electric Vehicles with Individually Controlled Motors: State-of-the-Art and Future Developments," World Electric Vehicle Journal, Vol. 5, pp. 617-628, 2012.

[11] S. Khosravani, A. Kasaiezadeh, A. Khajepour, B. Fidan, S.-K. Chen, B. Litkouhi, "Torque-Vectoring-Based Vehicle Control Robust to Driver Uncertainties," IEEE Transactions on Vehicular Technology, Vol. 64, Iss. 8, pp. 3359-3367, 2015.

[12] G. D Filippis, B. Lenzo, A. Sorniotti, P. Gruber, and W. De Nijs, "Energy-Efficient Torque-Vectoring Control of Electric Vehicles with Multiple Drivetrains," IEEE Transactions on Vehicular Technology, Vol. 67, No. 6, pp. 4702-4715, 2018.

[13] C. Chatzikomis, M. Zanchetta, P. Gruber, A. Sorniotti, B. Modic, T. Motaln, L. Blagotinsek, and G. Gotovac, "An Energy-efficient Torque-vectoring Algorithm for Electric Vehicles with Multiple Motors," Mechanical Systems and Signal Processing, Vol. 128, pp. 655-673, 2019.

[14] A. Parra, D. Tavernini, P. Gruber, A. Sorniotti, A. Zubizarreta, and J. Pérez, "On Nonlinear Model Predictive Control for Energy-Efficient Torque-Vectoring," IEEE Transactions on Vehicular Technology, Vol. 70, No. 1, pp. 173-188, 2021.

[15] X. Hu, H. Chen, Z. Li, and P. Wang, "An Energy-Saving Torque Vectoring Control Strategy for Electric Vehicles Considering Handling Stability Under Extreme Conditions," IEEE Transactions on Vehicular Technology, Vol. 69, No. 10, pp. 10787-10796, 2020.
[16] C. Lin, S. Liang, J. Chen, and X. Gao, "A Multi-Objective Optimal Torque Distribution Strategy for Four In-Wheel-Motor Drive Electric Vehicles," IEEE Access, Vol. 7, pp. 64627-64640, 2019.
[17] H. Fujimoto and S. Harada, "Model-Based Range Extension Control System for Electric Vehicles with Front and Rear Driving-Braking Force Distributions," IEEE Transactions on Industrial Electronics, Vol. 62, No. 5, pp. 3245-3254, 2015.
[18] Y. Wang, H. Fujimoto, and S. Hara, "Torque Distribution-Based Range Extension Control System for Longitudinal Motion of Electric Vehicles by LTI Modeling with Generalized Frequency Variable," IEEE/ASME Transaction on Mechatronics, Vol. 21, Iss. 1, pp. 443-452, 2015.
[19] Y. Ikezawa, H. Fujimoto, Y. Hori, D. Kawano, Y. Goto, M. Tsuchimoto, and K. Sato, "Range Extension Autonomous Driving for Electric Vehicles Based on Optimal Velocity Trajectory Generation and Front-Rear Driving-Braking Force Distribution," IEEJ Journal of Industry Application, Vol. 5, No. 3, pp. 228-235, 2016.
[20] X. Sun, C. Hu, J. Zhu, S. Wang, W. Zhou, Z. Yang, G. Lei, K. Li, B. Zhu, and Y. Guo, "MPTC for PMSMs of EVs With Multi-Motor Driven System Considering Optimal Energy Allocation," IEEE Transactions on Magnetics, Vol. 55, No. 7, Art No. 8104306, 2019.
[21] X. Zhang, D. D. Göhlich, and J. Li, "Energy-Efficiency Torque Allocation Design of Traction and Regenerative Braking for Distributed Drive Electric Vehicles," IEEE Transactions on Vehicular Technology, Vol. 67, No. 1, pp. 285-295, 2018.
[22] X. Zhang and D. Göhlich, "Integrated Traction Control Strategy for Distributed Drive Electric Vehicles with Improvement of Economy and Longitudinal Driving Stability," Energies 10, No. 1:126, 2017.
[23] B-M. Nguyen, J. P. Trovão, M. Ta-Cao, and M. Kawanishi, "Longitudinal Motion Control of Electric Vehicles: Glocal Model and Design Using Passivity," IEEE Vehicular Technology Magazine, Vol. 16, No. 3, pp. 75-86, 2021.
[24] H. B. Pacejka, "Tyre and Vehicle Dynamics," Elsevier BV, 2006.
[25] S. Morimoto, Y. Tong, Y. Takeda, and T. Hirasa, "Loss Minimization Control of Permanent Magnet Synchronous Motor Drives," IEEE Transactions on Industrial Electronics, Vol. 41, No. 5, pp. 511-517, 1994.
[26] R. Ortega, A. Loria, P. J. Nicklasson, and H. Sira-Ramirez, "Passivity-based Control of Euler-Lagrange Systems," Springer, 1998.
[27] B-M. Nguyen, M. Kawanishi, D. Hasegawa, K. Ohara, and T. Narikiyo, "Range Extension Control of a Three-Wheel Electric Vehicle Prototype Based on Aggregation and Distribution," IEEJ Journal of Industry Applications, Vol. 10, No. 5, 2021.
[28] J. Amada and H. Fujimoto, "Torque Based Direct Driving Force Control Method with Driving Stiffness Estimation for Electric Vehicle with In-wheel Motor," 38th Annual Conference on IEEE Industrial Electronics Society, pp. 4904-4909, 2012.
[29] H. K. Khalil, "Nonlinear Systems," Prentice Hall, 2002.
[30] E. Sariyildiz, R. Oboe and K. Ohnishi, "Disturbance Observer-Based Robust Control and Its Applications: 35th Anniversary Overview," IEEE Transactions on Industrial Electronics, Vol. 67, No. 3, pp. 2042-2053, 2020.
[31] Kun Jiang, A. Pavelescu, A. Victorino and A. Charara, "Estimation of vehicle's vertical and lateral tire forces considering road angle and road irregularity," International IEEE Conference on Intelligent Transportation Systems, pp. 342-347, 2014.
[32] K. Fujii and H. Fujimoto, "Traction Control based on Slip Ratio Estimation Without Detecting Vehicle Speed for Electric Vehicle," Power Conversion Conference, pp. 688-693, 2007.
[33] J. Lee, K. Nam, S. Choi and S. Kwon, "Loss-Minimizing Control of PMSM With the Use of Polynomial Approximations," IEEE Transactions on Power Electronics, Vol. 24, No. 4, pp. 1071-1082, 2009.
[34] A. Dianov, F. Tinazzi, S. Calligaro and S. Bolognani, "Review and Classification of MTPA Control Algorithms for Synchronous Motors," in IEEE Transactions on Power Electronics, vol. 37, no. 4, pp. 3990-4007, 2022.
[35] J. P. Trovao, M-A. Roux, E. Menard, and M. R. Dubois, "Energy and Power-Split Management of Dual Energy Storage System for a Three-Wheel Electric Vehicle," IEEE Transactions on Vehicular Technology, Vol. 66, Iss. 7, pp. 5540-5550, 2016.
[36] A. Van Der Schaft, "L_2-Gain and Passivity Techniques in Nonlinear Control," Springer, 2017.

Binh-Minh Nguyen (Member, IEEE) received his M.S and Ph.D. degrees from the University of Tokyo in 2012 and 2015. He is currently an Assistant Professor at Department of Advanced Energy, the University of Tokyo. His research interests include glocal control, passivity control, motion control, and their applications in electric vehicles, flying vehicles, and power systems. Dr. Nguyen was the recipient of Paper Awards in IEEE International Conference on Mechatronics 2015, and IEEE Vehicular Power and Propulsion Conference 2012. He was awarded the 2021 Kurata Grant and the 2022 Nagamori Grant. Dr. Nguyen is an Associate Editor for the Automotive Electronics topic of the IEEE Vehicular Technology Magazine. Since 2021, he has served as an Area Editor of the EAI Endorsed Transactions on Industrial Networks and Intelligent Systems.

João Pedro F. Trovão (Senior Member, IEEE) received the Ph.D. degree in Electrical Engineering from the University of Coimbra, Coimbra, Portugal, in 2013.

Since 2014, he has been a Professor with the Department of Electrical Engineering and Computer Engineering, University of Sherbrooke, Sherbrooke, QC, Canada, where he holds the Canadian Research Chair position in Efficient Electric Vehicles with Hybridized Energy Storage Systems. He is an author/coauthor of over 130 journal and conference papers. His research interests cover the areas of electric vehicles, hybridized energy storage systems, energy management and rotating electrical machines. Dr. Trovão was the General Chair of the 2018 IEEE Vehicle Power and Propulsion Conference, Chicago, US. He was a Guest Editor for the Special Issue of IET ELECTRICAL SYSTEMS IN TRANSPORTATION on Energy Storage and Electric Power Sub-Systems for Advanced Vehicles. He was a Guest Editor for the Special Issues of IEEE TRANSACTIONS ON VEHICULAR TECHNOLOGY on Electric Powertrains for Future Vehicles and on Advanced Vehicle Power Propulsion Systems. He is a founding member and the director of the electric-Transport, Energy Storage and Conversion (e-TESC) Lab of the University of Sherbrooke. He is a Senior Editor for the Automotive Electronics topic of the IEEE VEHICULAR TECHNOLOGY MAGAZINE.

Minh C. Ta (Senior Member, IEEE) received the B.S. (Hons.) degree from the Institute of Technology (now the University of West Bohemia), Pilsen, Czech Republic, in 1986, and the Ph.D. degree from Laval University, QC, Canada, in 1998, both in electrical engineering. From 1998 to 2004, he was with Kyushu University, Japan; The University of Tokyo, Japan; and NSK Steering Systems Ltd. Co., Japan. In 2009, he became an Associate Professor with the Hanoi University of Science and Technology (HUST), Vietnam, and was the Founding Director of the Center for Technology Innovation (CTI) 2009 – 2018, and Head of the Department of Industrial Automation, HUST, 2018 – 2020. He is currently with the Department of Electrical and Computer Engineering, University of Sherbrooke, Sherbrooke, QC, Canada. His main research interests include motor drives and advanced control techniques and their applications for electric vehicles and energy conversion systems. Dr. Ta received the Second Prize Paper Award of the Industrial Drives Committee of the IEEE Industrial Applications Society in 2001, and the Best Paper Award of the IEEE Vehicle Power and Propulsion Conference (VPPC) 2018. He was a recipient of the 2012 NSK Patent Awards and the 2017 Nagamori Awards. He was the General Chair of the IEEE VPPC 2019, Hanoi, Vietnam. He has been a Guest Editor of several Special Issues of the IEEE Transaction on Vehicular Technology since 2020.